Arabian Journal of Chemistry (2020) 13, 4629–4643

King Saud University

Arabian Journal of Chemistry

www.ksu.edu.sa
www.sciencedirect.com

ORIGINAL ARTICLE

Simultaneous adsorption of tetracycline, amoxicillin, and ciprofloxacin by pistachio shell powder coated with zinc oxide nanoparticles

Ahmed A. Mohammed [a], Tariq J. Al-Musawi [b,*], Sabreen L. Kareem [c], Mansur Zarrabi [d], Alaa M. Al-Ma'abreh [e]

[a] *Department of Environmental Engineering, College of Engineering, University of Baghdad, Iraq*
[b] *Department of Civil Engineering, Faculty of Engineering, Isra University, Amman, Jordan*
[c] *Environmental Planning Department, Physical Planning College, University of Kufa, Iraq*
[d] *Department of Environmental Health Engineering, Research Center for Health, Safety. Environment (RCHSE), Alborz University of Medical Sciences, Karaj, Iran*
[e] *Department of Chemistry, College of Science, Isra University, Amman, Jordan*

Received 6 September 2019; accepted 24 October 2019
Available online 12 November 2019

KEYWORDS

Adsorption;
Antibiotics;
ZnO;
Simultaneous;
Competitive;
Characterization

Abstract A new adsorbent formed from pistachio shell powder that was coated with ZnO nanoparticles (CPS) was examined in terms of simultaneous adsorption of tetracycline (TEC), amoxicillin (AMO), and ciprofloxacin (CIP) from an aqueous solution. Initially, the characterization properties of a CPS-like surface morphology, functional groups, and structure were obtained using advanced analysis of TEM, SEM, XRD, EDS, and FT-IR. Post coating with ZnO nanoparticles, several surface and structural characteristics relating to the adsorption ability of the pistachio shell were significantly improved. The correlation of the kinetic data by a pseudo second-order model was successful for three antibiotics. High compatibility resulted between the TEC and CIP isotherm data and the Fruendlich model. However, the Langmuir model produced a better fit to the AMO isotherm curves. In addition, its spontaneous and exothermic nature was the main feature for the adsorption process of the three antibiotics onto CPS. Through the results, the chemical adsorption has been governed by the AMO, CIP, and TEC reaction onto the homogeneous and heterogeneous sites of CPS surfaces. The CPS exhibited a highest adsorption capacity for AMO (132.240 mg/g), then for TEC (98.717 mg/g), and CIP (92.450 mg/g). These results place CPS

* Corresponding author.
E-mail address: tariq.almusawi@iu.edu.jo (T.J. Al-Musawi).
Peer review under responsibility of King Saud University.

Production and hosting by Elsevier

https://doi.org/10.1016/j.arabjc.2019.10.010

one among the highly efficient adsorbents that can be used to eradicate wastewater containing antibiotics.

1. Introduction

At the present time, pollution of water resources by pharmaceutical wastes is one of the greatest and serious environmental challenges facing communities, especially in places where there is reliance on these sources for drinking purposes (Gasser et al., 2008; Oh et al., 2017). Excessive pharmaceutical compounds in environmental matrices are classified as hazardous materials that can damage the natural ecosystem by changing the status of the equilibrium (Kalhori et al., 2018; Ji et al., 2014). These chemicals can enter the aquatic bodies including surface and ground water through various anthropogenic activities, such as, waste streams from hospitals and pharmaceutical and veterinary industries, from their manufacture to disposal (BIO Intelligence Service, 2013). Antibiotics are a part of pharmaceutical compounds, which are consumed in great quantities, as they are highly effective in treating a wide spectrum of bacterial diseases in humans, livestock, poultry, and fish (Soori et al., 2016; Huang et al., 2017; Hassani et al., 2014; Legnoverde et al., 2014). Among the various types of antibiotics; tetracycline, amoxicillin, and ciprofloxacin are widely used in the world as efficacious therapeutic agents in the treatment of a variety of bacterial diseases (Al-Musawi et al., 2019; Mohammed and Kareem, 2019; Samarghandi et al., 2015). The discharge of pharmaceutical wastewater loaded with antibiotics can cause lethal health risks to non-target humans and biota, related to their chronic or acute exposure, as they contain toxic and carcinogenic elements. Besides, they may cause fetal abnormalities (Shi et al., 2019; Bondarczuk and Piotrowska-Seget, 2019; Pouretedal and Sadegh, 2014). From another side, various studies have reported that the disinfection of by-product chemicals, which are considered as carcinogenetic agents, were detected in the final treating stages due to the chlorination of wastewater containing antibiotics. Therefore, there is an urgent need to reduce the antibiotic compounds to the permissible limits prior to being discharged into water bodies (Balcioglu and Otker, 2004). Without a doubt, antibiotics are characterized by their stability in the environment and their long degradation time. Moreover, they are not completely removed using conventional treatment methods (Xian et al., 2010; Davis et al., 2003). With regard to the last point of characterization, an efficacious and advanced technology has to be applied to treat wastewater containing antibiotics. One of the most interesting treatment methods is the adsorption process (Al-Musawi et al., 2018; Zou et al., 2019).

The adsorption treatment method is an efficient, simple, and universal advanced treatment technology. This treatment method employs using natural or synthesized material (known as sorbent, adsorbent, or biosorbent) for the abatement of pollutant molecules (known as adsorbates) from contaminated solutions (Zou et al., 2019; Ahalya et al., 2003; Al-Musawi et al., 2018). For the adsorption process to be integrated in terms of removal efficiency and economic feasibility, the adsorbent should be chosen with great care (Gisi et al., 2016; Ghorai et al., 2014). In this context, the adsorbents should be tested for their adsorption performance toward numerous contaminants before being applied. Additionally, these tests should take into consideration the availability and cost-effectiveness of the tested adsorbents (Cheng et al., 2019; Wang et al., 2018). In recent times, agricultural waste, in its original or modified form, has attracted a great deal of attention by the scientific workers, to be utilized as adsorbents (Kamar et al., 2017; Sulaymon et al., 2014; Hossain et al., 2012). This is because of their low cost, availability in large quantities, and also they are found to be efficient for removal of several organic and inorganic matters in the adsorption systems (Khodadadi et al., 2019; Holan and Volesky, 1995). To further improve the adsorption capacity of agricultural wastes and to enhance their practical performance, some surface modifications have been suggested. For example, different particles of nano size have been successfully used for coating the surfaces of several adsorbents. The result of this modification was the formation of a more effective adsorbent (Mohammed et al., 2018; Dhiman and Sharma, 2018).

Zinc oxide nanoparticles were examined and studied by several adsorption studies and they successfully passed the tests and were selected as adsorbents and catalysts in the treatment systems (Bazrafshan et al., 2019; Zhang et al., 2016). ZnO is easy to manufacture, cheap, has an adjustable morphology, is eco-friendly, and it is not affected by any change in the environmental conditions (Li et al., 2017). In addition, the isoelectric point of ZnO is high and equal to 9.5, which improves the positive charge of its surface (Bazrafshan et al., 2019; Joshi, 2018; Wang et al., 2016). Of late, ZnO nanoparticles have been used to coat various dry adsorbents such as mesoporous silica (Jeong et al., 2014), zeolite (Wang et al., 2016), cross-linked chitosan/polyvinyl alcohol microspheres (Abdelwahab and Ghoneim, 2018), 13X zeolite, activated carbon (Changsuphan et al., 2012), and SiO_2 nanoparticles (Zhang et al., 2016), with good results being demonstrated.

Agriculture waste, such as a pistachio shell (PS), provides an effective surface for coating with ZnO nanoparticles, which is the goal of this research. Moreover, ZnO nanoparticles are promising agents in the adsorption systems. Pistachio shells, similar to other agricultural materials, are comprised of a number of functional groups having a negative charge, such as, polysaccharides and carbohydrates. These groups have a high tendency to bond with the positive charge of the ZnO particles (Piness, 2010; Hashemian and Shayegan, 2014). To date, using pistachio shell powder coated with ZnO nanoparticles (CPS) as an adsorbent agent for the remediation of pharmaceutical wastewater has not been reported. Moreover, it is important, in the adsorption studies, to investigate the mechanism of competition removal of several antibiotics in the adsorption treatment process. This is mainly because of the analysis of wastewater samples taken from the effluents from hospitals and drugs factories, which showed that various antibiotics can be present simultaneously in this wastewater (Lien et al., 2016; Binh et al., 2018). Therefore, the present research aims

to prepare and characterize the CPS. Later, the adsorption performance of the CPS toward simultaneous removal of tetracycline (TEC), amoxicillin (AMO), and ciprofloxacin (CIP) antibiotics is studied in detail, where the effect of some environmental parameters on the adsorption behavior are taken into consideration.

2. Materials and methods

2.1. Chemicals

Powdered TEC hydrochloride (chemical formula: $C_{22}H_{24}O_8N_2.HCl$, molecular weight: 480.9 g/mol, and purity: 98%), AMO (chemical formula: $C_{16}H_{19}N_3O_5S$, molecular weight: 365.4 g/mol, and purity: 97.5%), and CIP hydrochloride (chemical formula: $C_{17}H_{19}ClFN_3O_3$, molecular weight: 367.8 g/mol, and purity: 99%) were obtained from a general company in the drugs industry (Samarra, Iraq) without further purification (original manufacturer: Merck, Germany). Fig. 1 shows the chemical structures of these three antibiotics. The ternary stock solution of TEC, AMO, and CIP of 500 mg/L each, was prepared by dissolving an appropriate quantity of powdered antibiotics in 1 L of deionized water. To get a homogenous solution, the stock solution was vigorously stirred for 30 min, thereafter, the working solutions were prepared by dilution. On account of the instability in the laboratory conditions, the stock and diluted solutions were prepared at the time of the experimental study. The pH value of the solutions was controlled during the experiments by addition of the buffer solution dropwise.

2.2. Synthesizing of the CPS

In the present study, the target adsorbent of CPS was prepared in the laboratory according to the following basic methodology. Initially, a certain quantity of pistachio shells was collected from the flour mills. Then, it was subjected to the following steps: washing with deionized water, oven drying at 105 °C overnight, grinding, and sieving. The quantity of retained powder on mesh No. 200 was collected and kept in an appropriate container. On the other hand, 300 g of ZnO nanoparticles were purchased from Xi'an Lyphar Biotec (China). The obtained ZnO nanoparticles were dispersed thoroughly in acetone under a sonolysis process for 30 min. Following this, the powdered pistachio shells were added to the ZnO nanoparticles solution at a ratio of 5:1 (g/g) and vigorously stirred until a homogenous mixture was obtained. Next, the liquid was decanted and the resulting precipitate of CPS was filtered, and placed in an oven at 60 °C until complete dryness. Finally, the dried CPS was stored in flasks with stoppers to be used in the required experiments.

2.3. Characterizations

An X-ray diffractometer (XRD, Philips-Magix Pro MPD, Netherlands) was used to obtain the XRD patterns of the crystalline structure of CPS. These patterns were collected in a range of 2θ, from 5° to 60°, with a step width of 0.02° and scan rate of 1° per second. Scanning electron microscopy (SEM) images were taken using the SEM device (TESCAN-Vega3, Czech Republic). These images helped to detect the changes in the surface morphology that occurred due to adsorbent synthesizing or due to the adsorption process. The elemental composition of CPS was obtained using EDS analysis technique. Furthermore, to identify the surface morphology and size of the ZnO nanoparticles, a Philips-CM30 scanning transmission electron microscopy (TEM, Netherlands) was used for taking a TEM image. A Shimadzu FTIR spectroscopy instrument (Japan) was used to detect the functional groups existing on the CPS and their significance in the removal process. Notably, these analyses were carried out within the wave number region of 500–4000 cm^{-1}, as all the well-known groups of agricultural adsorbents fell within this range. The specific surface area of PS and CPS was determined using Brunauer–Emmett–Teller (BET) analysis. For this test, a CPS sample of 120 mg was transferred to the BET holder tube (inner diameter = 0.7 cm) and degassed at temperature of 150 °C for 4 h, under vacuum, before analysis. Moreover, the pH of the zero point of charge (pHzpc) of CPS was determined according to the method described in the article by Mohseni-Bandpi et al., (2016). This test, in fact, was essential to identify the type of CPS surface charge, with respect to the pH of the solution.

2.4. Adsorption experiments

The adsorption experiments in this study were performed in a batch-ternary system of three antibiotics. The experiments in this study were conducted using varying factors: pH (3–9);

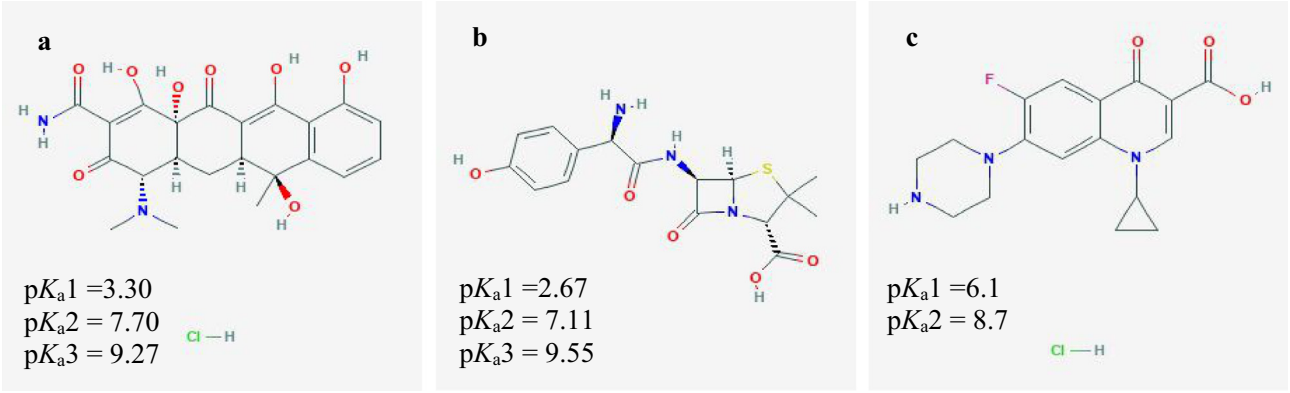

Fig. 1 The chemical structure of TEC (a); AMO (b) CIP, and (c) antibiotics (Ghadim et al., 2013; Sharma et al., 2009).

adsorbent dose (0.02–1 g/100 mL antibiotic solution); contact time (0–120 min); initial antibiotic concentration (30–70 mg/L), and temperature (25–35 °C). For this purpose, several flasks of 500 mL were filled with 100 mL solution containing 100 mg/L of a mixture of TEC; AMO, and CIP antibiotics. The antibiotic solutions in each flask were mixed with CPS of dose = 0.1 g/100 mL (expect in the adsorbent dose experiment) and shaken for an equilibrium time, as determined from a contact time experiment, and at a constant shaking speed of 150 rpm. The optimized value of each parameter, in which the highest adsorption capacity was recorded, was used in the subsequent experiment. At different time intervals during the adsorption experiments, three replicates of samples, of 3 mL each, were taken out from each flask and analyzed for the remaining antibiotic concentrations. The initial and remaining TEC; AMO, and CIP concentrations were determined according to the calibration data that were obtained by using UV/VIS spectrophotometers, with an absorbency reading of peak wavelengths at 360; 272, and 276 nm, respectively. It is worth noting that the adsorption data of the effects of temperature, contact time at different initial concentrations values, and adsorbent dose, were utilized in the thermodynamic, kinetic, and isotherm studies, respectively. The ability of the CPS to remove the antibiotic pollutants from aqueous solutions was judged according to the values of the removal efficiency ($R\%$) and adsorption capacity (q_e, mg/g) (Noroozi et al., 2018; Mohseni-Bandpi et al., 2016), which are calculated by the following two formulae:

$$R\% = \frac{(C_0 - C_t) \times 100}{C_0} \quad (1)$$

$$q_e = \frac{(C_0 - C_e) \times V}{W} \quad (2)$$

where, C_0;C_t, and C_e denote the 'initial', 'after specific time of adsorption', and 'equilibrium' concentrations of antibiotics in the aqueous phase (mg/L), respectively, V is the volume of the antibiotic solution in (L), and the quantity of the used CPS adsorbent (g) is denoted by W in Eq. (2).

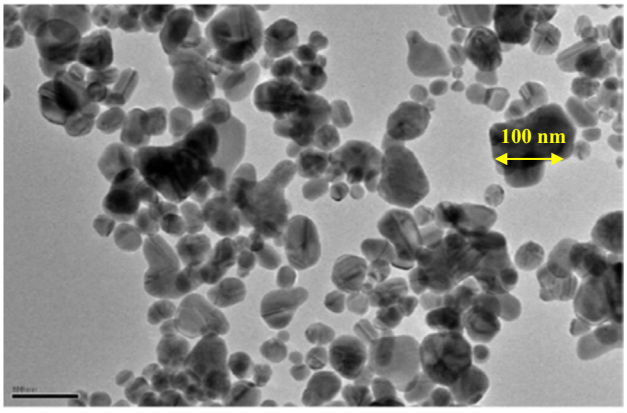

Fig. 2 TEM image of ZnO nanoparticles.

3. Results and discussion

3.1. Characterization of ZnO, PS, and CPS

A high resolution TEM image (Fig. 2) showed that the ZnO nanoparticles have an irregular shape, but most of them are roughly spherical with an average size of <100 nm. Thus, these particles are within the nano-size range. Also, the agglomeration of these nanoparticles is low, as their dispersion appears to be in a mono-dispersed manner. This is a positive adsorptive characteristic for ZnO nanoparticles, as the mono-dispersed particles offer a maximum benefit from the surface area that is allocated for adsorption of the pollutant molecules, rather than multi-dispersed particles (Bazrafshan et al., 2019; Chen et al., 2011). Therefore, ZnO can be a promising material for coating of adsorbents with low adsorption capacity.

The typical SEM micrographs of PS and CPS before and after simultaneous adsorption of TEC, AMO, and CIP molecules are presented in Fig. 3. Clearly, the morphological characteristics of PS (Fig. 3a) are completely changed after coating

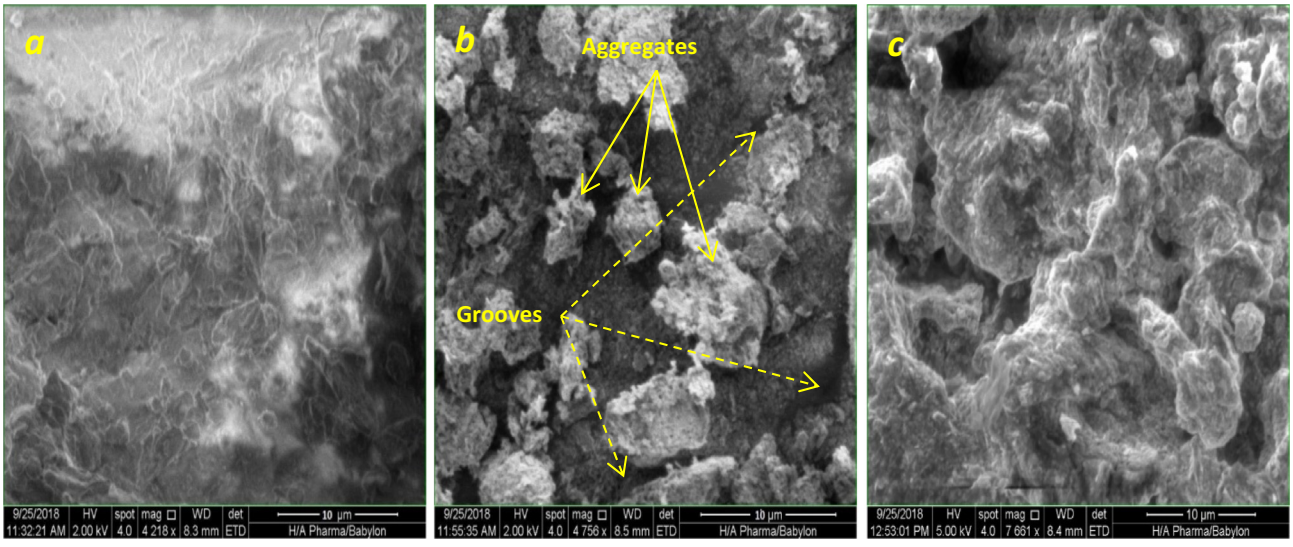

Fig. 3 SEM micrographs of PS (a) and CPS before (b), and after (c) simultaneous adsorption of TEC; AMO, and CIP molecules.

with ZnO nanoparticles as seen in Fig. 3b. The SEM of the CPS indicates that the surface of this adsorbent is coarse; as well as it consists of several non-uniform and separated aggregates. In addition, there are many big ravines and long grooves in the outer wall of CPS. In fact, these morphological properties of the CPS surface represent a positive point, as they provide a high surface area and active sites for sorbing the adsorbate molecules. In this manner, the specific surface area of PS has been determined to be 0.97 m^2/g, which significantly increases to 4.24 m^2/g, after coating with ZnO nanoparticles. On comparing Fig. 3b and the SEM image of CPS after adsorption (Fig. 3c), it can be seen that the morphological properties of CPS are significantly altered during the simultaneous antibiotic adsorption. Noticeably, the surface of CPS becomes smoother, and several pre-separated aggregates are coalesced. This situation appeared as a result of adsorption of three antibiotics on active sites of the CPS.

According to the FT-IR analysis of the raw PS sample (Fig. 4a), the presence of fats in this agricultural material is generally detected by bands of aliphatic C—H, stretching in the range of 3000–2800 cm^{-1} and C═O bonding in the range of 1745–1725 cm^{-1}. Although, carbohydrates have defining bands in the range of 1400–800 cm^{-1}, due to bonds between the glucose polymer chains (Stuart, 2004). In fact, the pistachio

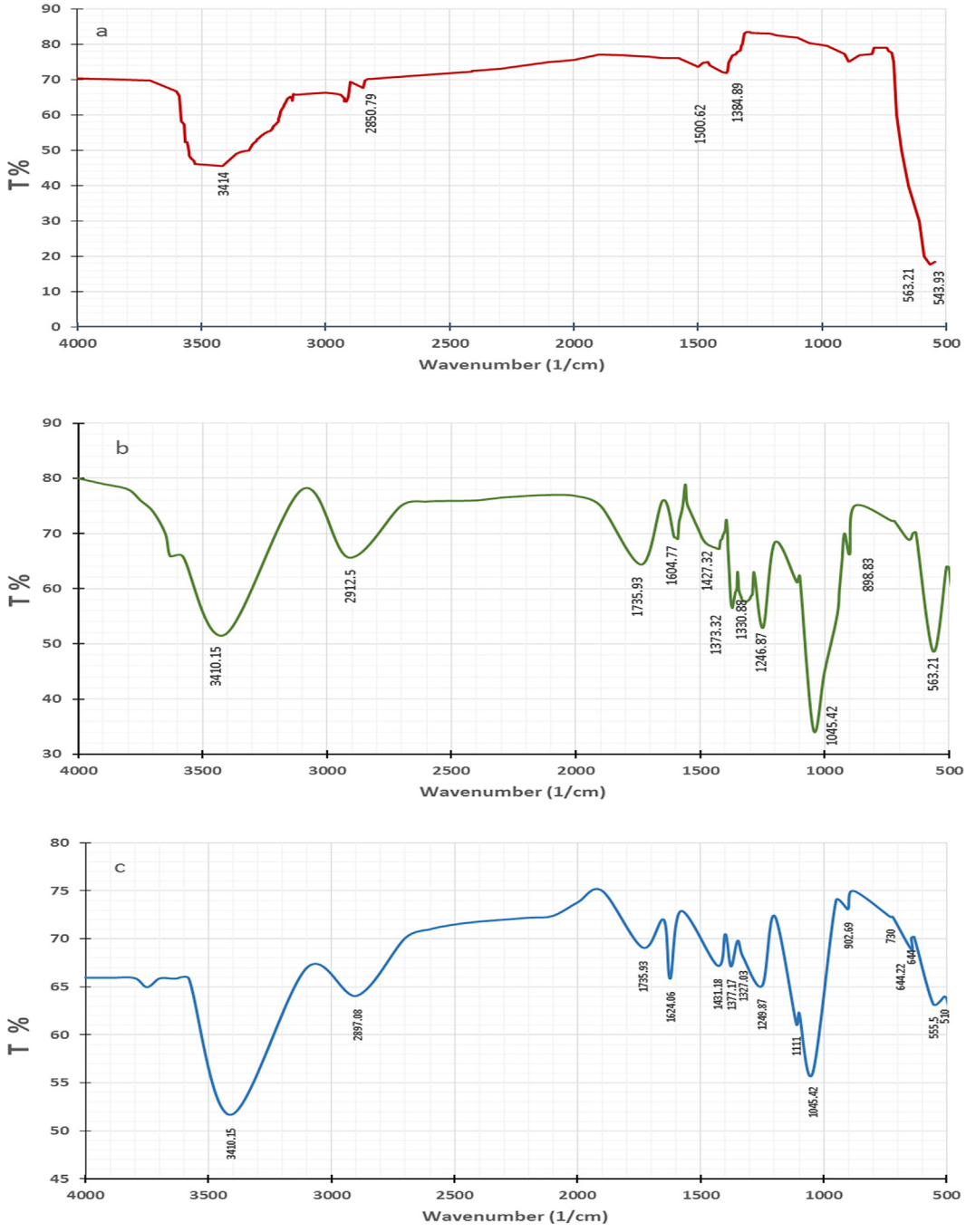

Fig. 4 FT-IR analysis of PS (a), and CPS before (b), and after (c) simultaneous adsorption of TEC; AMO, and CIP molecules.

FT-IR spectrum consists of four functional groups of importance in the present study (see Fig. 4a). The broad band detected at 3414 cm^{-1} is assigned to the O—H bond of alcohol. The band detected at 2929.09 cm^{-1} is attributed to the appearance of a C—H bond stretching functional group. The two bands at 1500.62 and 1384 $cm^{-1}$are related to bonds between polymer chains. Finally, the band at 894.97 cm^{-1} is assigned to vibrations of benzene and its derivatives (Piness, 2010). These groups offer effective sites for adhering ZnO nanoparticles. Fig. 4b is the result of the FT-IR analysis of CPS. Generally, the metal oxides demonstrate absorption bands in the FT-IR spectrum curve below 1000 cm^{-1} (Kumar and Rani, 2013). In this context, the band at 563.21 cm^{-1} corresponds to inorganic ZnO stretching (Handore et al., 2014). Compared to the spectrum of PS (Fig. 4a), there are obvious shifts in the CPS FT-IR bands (Fig. 4b) to new values: 3410.15, 2912.51, 1427.32, 1373.32, and 898.83 cm^{-1}, and this can be attributed to interactions between raw PS and the coating nanoparticles of zinc oxide nanoparticles. Also, the appearance of bands at 1735.93 cm^{-1} belongs to the ν(C═O) vibration in the carbonyl group or carboxylic bonds. The occurrence of this group is probably from the reactive carbon-containing plasma groups, which are used during the synthesizing processes of ZnO nanoparticles (Rana et al., 2012). The band at 1604.77 cm^{-1} is attributed to the presence of a C═O ring or a C═C stretching of aromatic groups. The absorption of the two bands detected at 1330.88 and 1045.02 cm^{-1} correspond to the stretching vibration of the C—H and C—O groups of alcohol, respectively (Rana et al., 2012). Fig. 4c represents the FT-IR spectrum for CPS after the adsorption process of three pharmaceutical products. On comparing between the FT-IT spectrum for CPS before (Fig. 4b) and after (Fig. 4c) the adsorption process, it is obvious that the intensity of the band at 3410.15 in Fig. 4b is slightly increased. This is due to the overlapping of the —OH and $—NH_2$ stretching vibrations by the pollutant molecules. In addition, bands observed at 1604.77, 1427.32, 1373.32, 1330.88, 1246.02, 898.83, and 555.5 cm^{-1} are shifted to new locations, which suggest the involvement of these functional groups in the sorbing of pollutant molecules. Weak bands at 1111 cm^{-1} are assigned to O-H stretching and deformation, which indicate the adsorption of water or a hydroxyl group on the metal surface of CPS (Rana et al., 2012). Moreover, absorption bands near 555.5 and 644.28 cm^{-1} normally correspond to ZnO stretching vibrations (Kumar and Rani, 2013). It can be seen that the band corresponding to ZnO ($< 1000\ cm^{-1}$) was still exist in the FT-IR spectrum of the CPS after adsorption. This finding suggests that the ZnO nanoparticles are still attached onto PS surface during the adsorption process.

The results of XRD analysis of PS and CPS in the range of 5°–60° are presented in Fig. 5. It can be seen that the dominant material in the crystallographic structure of PS (Fig. 5a) is silica, as SiO_2 compounds present naturally in PS. It is worth mentioning that similar to many agricultural materials, PS in its internal structure, is naturally rich in minerals such as zinc and magnesium (Ghaseminasab et al., 2015), so these elements appear in small traces in the PS XRD pattern. In the XRD spectra of CPS (Fig. 5b), additional peaks are observed after PS is coated with ZnO nanoparticles. The sharp peaks observed in the range of 30°–40° are associated with zinc of high quantity, confirming its existence as a PS coating layer (Bazrafshan et al., 2019).

The elemental composition of CPS prior and post adsorption reactions with three antibiotics was obtained by capturing the EDS spectrums (Fig. 6). Clearly, the elements which appeared in the EDS spectrum of CPS before the adsorption are Mg, Si, C, Ca, and F. In addition, the mass ratio of Zn and O elements was high, which highlighted the successful interaction and shell of PS with ZnO nanoparticles. In addition, the Zn is also detected in the EDS spectrum of CPS after reaction. This confirms the stability of ZnO nanoparticles onto the CPS surface after adsorption process.

3.2. Adsorption mechanism

3.2.1. Effect of pH

In general, the removal efficiency of any pollutant in the adsorption system is dependable on the surface characteristics of the used adsorbent and speciation of the adsorbate, at specific pH values. In this case, the analysis of pH_{pzc} is very important, to indicate the pH value at which the surface of the adsorbent is of neutral charge. In other words, the surface charge of the adsorbent is negative when the pH values are higher than pH_{pzc} and vice versa (Sun et al., 2016). On the other hand, at different pH values the adsorbate molecules may have different surface charges, which greatly affect their tendency toward adsorbent particles. The variation in the removal percent of TEC, AMO, and CIP as a function of pH and contact time are displayed in Fig. 7. Clearly, the amount of each antibiotic adsorbed onto the CPS in the ternary system increases, showing a pH increase from 3 to 5, and subsequently it decreases with the increase of pH. Such adsorption behavior can be explained according to the electrostatic interactions between antibiotic molecules and surface of the CPS. For example, the TEC molecule has several ionizable functional groups like dimethyl ammonium, tricarbonyl amide, and phenol diketone groups. These active groups undergo protonation–deprotonation reactions, as a result they may be formation of a species of H_2TEC^+ at pH < 3.3. While, the zwitterion species of H_2TEC^0 are formed in case the pH of the solution ranges from 3.3 to 7.7. At pH > 7.7, anion species of $HTEC^-/TEC^{2-}$ are dominant in the aqueous solution (Hsu et al., 2018). According to the analysis, the pH_{pzc} of the CPS was determined to be 6.5. Also, it is important to note that the surface of the ZnO nanoparticle typically comprises of hydroxyl (OH) groups of neutral charge. The charge of this group may vary according to the pH value (Qu and Morais, 1999; Qu and Morais, 2001). At pH > pH_{pzc}, the H^+ ions leave the particle surface owing to a negative charge of ZnO with partially bonded oxygen atoms, that is, ZnO^-. Conversely, at pH < pH_{pzc}, ions of H^+ are transferred to the particle surface and combined with the OH^- groups leading to a positive charge of the ZnO surface due to formation of $ZnOH_2^+$ groups. Under these circumstances, the net surface charges of the ZnO nanoparticles and CPS at pH = 5 are positive, thus electrostatic attraction may take place among them and the negatively charged tricarbonylamide groups of TEC, which results in high TEC removal efficiency. When the pH is below 5, the electrostatic repulsion between the positively charged ZnO nanoparticles and cationic moieties of TEC causes a decrease in the TEC adsorption efficiency. Similar results were obtained in the case of AMO adsorption onto CPS. For CIP adsorption, it is known that the molecules of

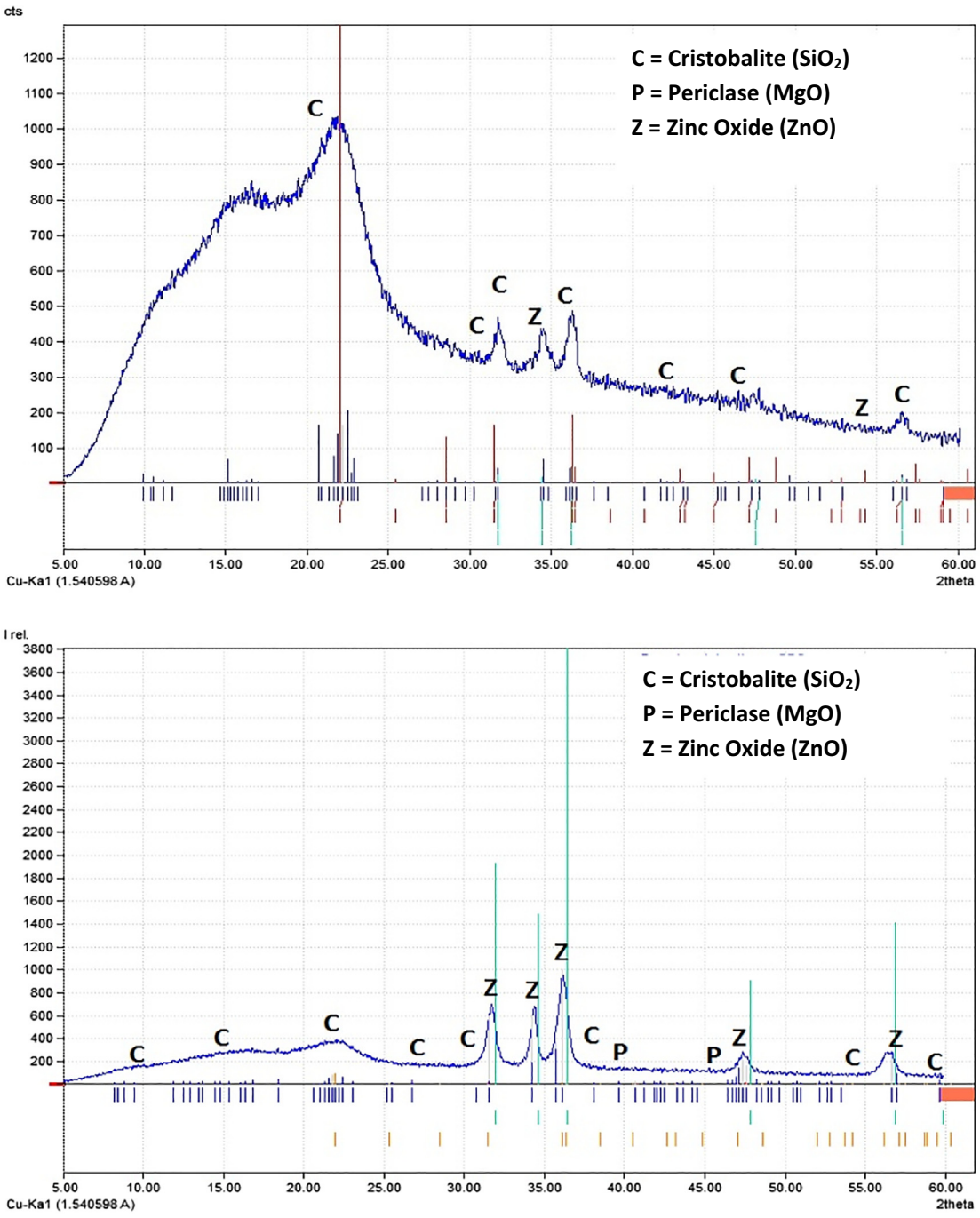

Fig. 5 XRD spectra of PS (a) and CPS (b).

this antibiotic are positively charged at aqueous solutions of pH lower than 4 where about 99% of the CIP molecules exist as CIP^+ (cationic), while at a pH higher than 10, over 95% of CIP molecules are present in a CIP^- form (anionic). At the pH = 7, the CIP^0 (zwitterion) is dominant within the system (Wu et al., 2010). It is observed that CIP adsorption is favored wherever the dissimilarity of adsorbents and CIP molecules charges occur. This is mainly due to the fact that when the adsorbate molecules and adsorbent surface have dissimilar charges, electrostatic attraction forces tend to exist, which can benefit the adsorption process. Therefore, a chemisorption reaction may occur between the CIP molecules and CPS active sites at pH = 5.

3.2.2. Effect of contact time

In addition to the effects of the pH solution, the results plotted in Fig. 7 also show the simultaneous effect of an increase in the contact time. The removal efficiencies of three antibiotics presented in the ternary system increase with prolonged contact time and then they reach plateau adsorption within the first 30 min for TEC and CIP, and 60 min for AMO. For all the results recorded during the first 30 min of contact time, the

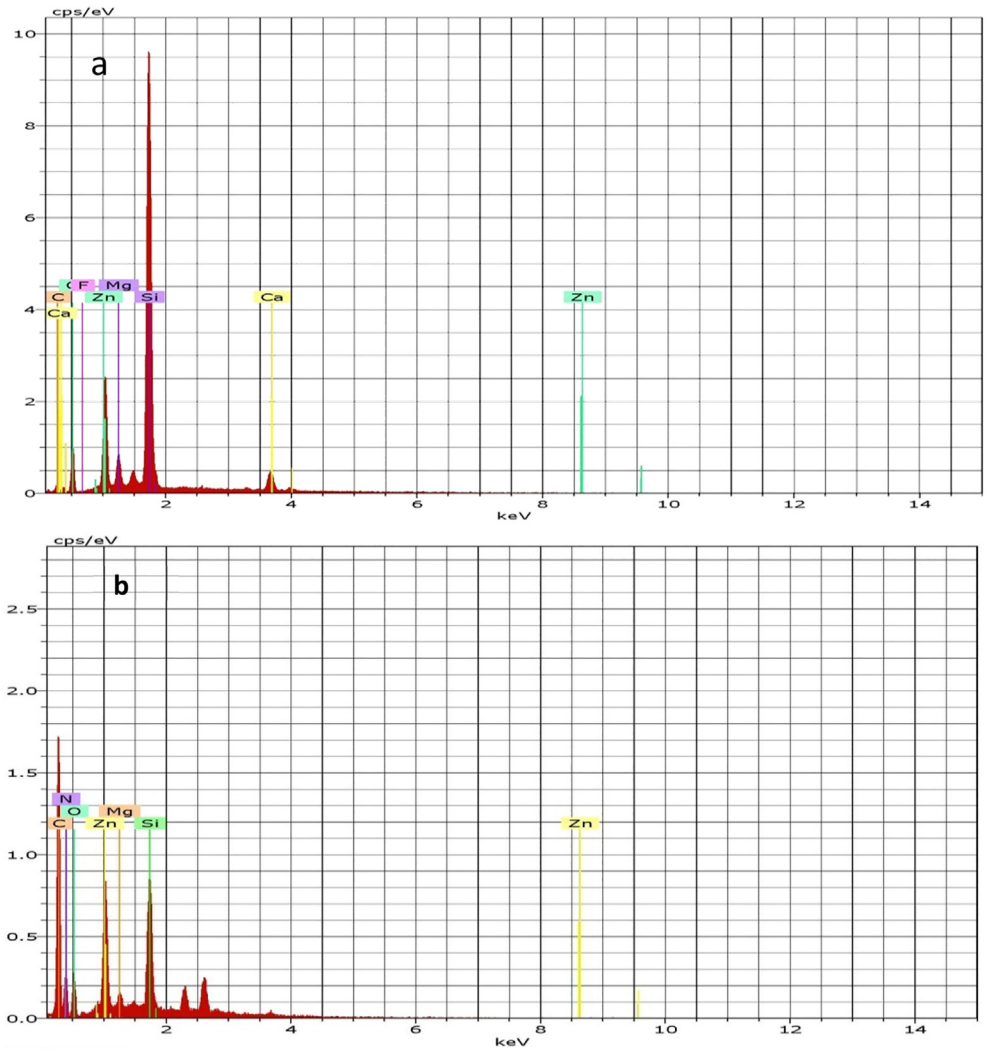

Fig. 6 EDS spectra of CPS before (a) and after (b) adsorption process.

removal rate of TEC, AMO, and CIP has been fast, and this can be attributed to the abundance of uncovered adsorption sites on the used adsorbent that are not occupied by contaminant molecules. In fact, the rapid pollutant removal by the applied adsorbent is considered as a positive property. Therefore, such adsorbents are good agents in the adsorption treatment processes. Subsequently, as the contact time moves from 60 to 120 min, the removal rate will slow down for all pH values. This phenomenon can be accounted as being due to the continuous decrease in both the adsorbent reaction sites and the concentration of non-adsorbed or non-reacted molecules of TEC, AMO, and CIP, until that moment, thus the removal percentage of antibiotic molecules increases slowly. The highest removal of TEC, AMO, and CIP efficiencies is reached at pH = 5 and a contact time of 120 min can be ranked as: CIP > TEC > AMO. The obtained results are compared with other similar researches (Mohammed et al., 2019; Abdelkareem *et al.,* 2019) and are found to be alike.

3.2.3. Thermodynamic study

The antibiotic removal efficiency was examined as a function of temperature from 25 °C to 35 °C and the results are depicted in Fig. 8. This figure indicates that the increase in temperature had minimal impact on the adsorption ability of CPS for the three antibiotics. However, the removal efficiencies of three antibiotics were slightly decreased with the increase in the temperature. Indeed, the increase in the temperature will decrease the viscosity of the aqueous solution bearing the pollutant molecules which in turn permits the increase of diffusion rate of the adsorbate across the bulk (external) and pore (internal) boundaries of the adsorbent particles (Mohammed et al., 2019).

To investigate the thermodynamic analysis of CPS for simultaneous adsorption of TEC; AMO, and CIP, the thermodynamic parameters of Gibbs free energy change ($\Delta G°$, kJ/mol); surface adsorption of entropy change ($\Delta S°$, kJ/mol K), and enthalpy change ($\Delta H°$, kJ/mol) were calculated using the following equations (Khodadadi et al., 2019):

$$\Delta G^{\circ} = -RTln(k_d) \tag{3}$$

$$ln(k_d) = -\frac{\Delta H^{\circ}}{RT} + \frac{\Delta S^{\circ}}{R} \tag{4}$$

$$\text{With } k_d = \frac{q_e}{C_e} \tag{5}$$

where K_d (L/g) is the equilibrium constant which is equal to the ratio of the sorbed quantity of adsorbate molecules onto the

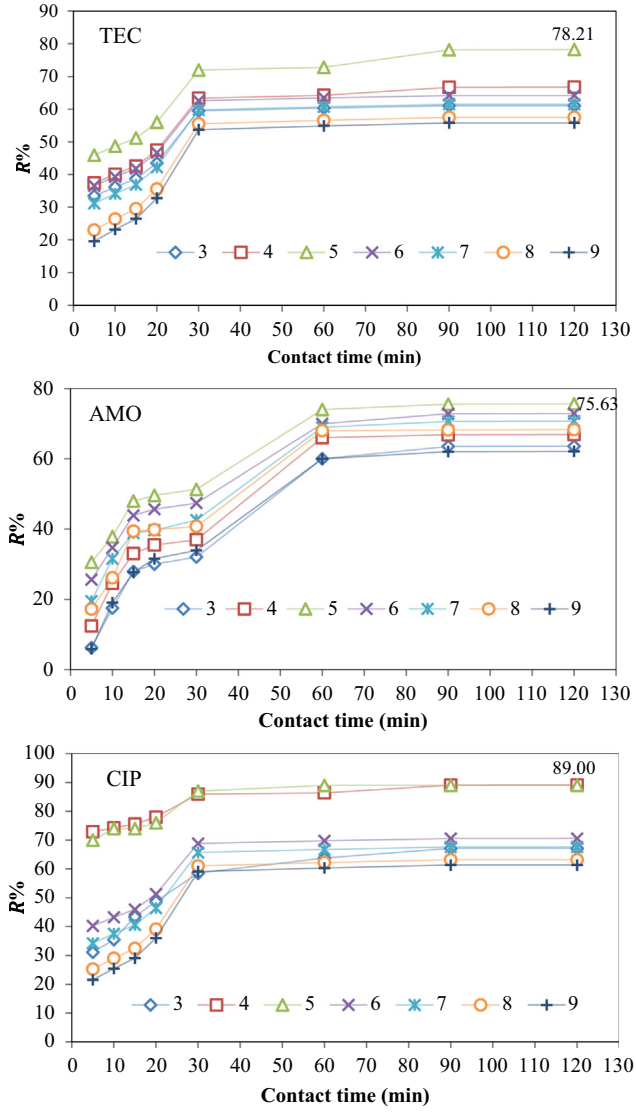

Fig. 7 Effect of pH on the TEC, AMO, and CIP adsorption efficiency onto CPS in the ternary system (initial antibiotic concentration = 60 mg/L, temperature = 25 ± 2 °C, agitation time from 0 to 120 min, agitation speed = 150 rpm, adsorbent dose = 0.1 g/100 mL).

adsorbent particles (mg/g) and the equilibrium adsorbate concentration (mg/L), T (K) is the solution temperature, and R is the universal gas constant (8.314×10^{-3} kJ/K mole).

In the present study, the thermodynamic analysis was conducted based on the obtained data of Fig. 7, and the results of this analysis are tabulated in Table 1. It can be evidenced that the adsorption reactions of the TEC, AMO, and CIP adsorption onto CPS was spontaneous, as negative values of ΔG° were determined for all the temperatures. Although, the negative values of ΔH° and ΔS° demonstrated that the nature of the adsorption was exothermic, and there was a decrease in randomness occurring during the reaction of TEC; AMO, and CIP with the CPS particles.

3.2.4. *Effect of antibiotic concentration and kinetic study*

The effect of the initial TEC, AMO, and CIP concentrations varied from 30 to 60 mg/L and their removal percentage by

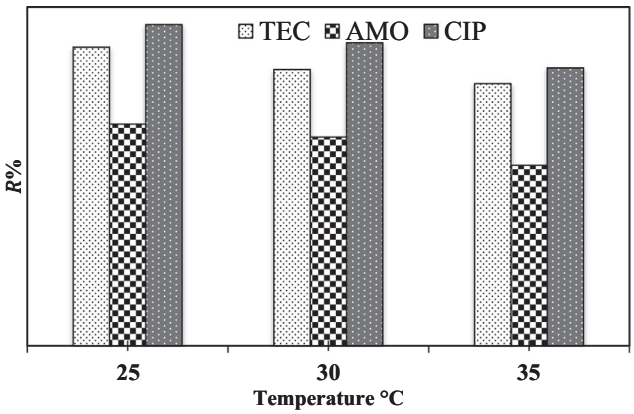

Fig. 8 Effect of temperature on the TEC, AMO, and CIP adsorption efficiency in the ternary system (initial antibiotic concentration = 60 mg/L, CPS dose = 0.1 g/100 mL, agitation time = 120 min, agitation speed = 150 rpm, pH = 5).

CPS was further tested. These experiments were conducted under environmental conditions: pH = 5; CPS dose = 0.1 g/100 mL; contact time = 0 to 120 min; agitation speed = 150 rpm, and temperature = 25 ± 2 °C. The evolution curves of the removal efficiencies depicted in Fig. 9 (a to c), demonstrated that the removal efficiencies of TEC, AMO, and CIP increased remarkably with an increase in the initial concentration. This was due to the high concentration gradients that formed at higher adsorbate concentrations (Gupta et al., 2017). The same explanation above was mentioned in the Arami et al. (2005) study.

The adsorption kinetics study is a very important stage for any practical application of adsorption treatment systems (Brouers and Al-Musawi, 2018). This is due to the obtained kinetic results that provide valuable insights into the reaction types and pathways, and the mechanism of pollutant removal. As a result, the design, operation, and control of the treatment process depend largely on the results of the kinetic study. In this manner, there is a necessity that highlighted the need for the experimental kinetic data to be properly modeled and fitted with the relevant kinetic models, in order to have an accurate design of the treatment system (Brouers and Al-Musawi, 2018). In this study, the two kinetic models of pseudo-first-order (Eq. (6)) and pseudo-second-order (Eq. (7)) were used to model the kinetic data of TEC; AMO, and CIP adsorption onto CPS. These models are widely applied in literature for modeling of the adsorption data of inorganic and organic pollutant removal from water solutions. The parameters of each model with their corresponding coefficient of regression values are determined using nonlinear fitting algorithms using a MATLAB program, the results are tabulated in Table 2. Based on the R^2 values, one can infer that the pseudo-second-order model was best-fitted equation for TEC; AMO, and CIP adsorption kinetic onto CPS. In addition for the pseudo-second-order model, a small deviation between the experimental and calculated uptake values, was determined. This finding indicates that the adsorption process of the TEC, AMO, and CIP, using CPS is chemical in nature (Mohammed et al., 2019; Aljeboree et al., 2017). Furthermore, in order to account for the contribution of intra-particle diffusion mechanism in all the kinetics of TEC, AMO, and CIP adsorption processes,

Table 1 Thermodynamic analysis of the simultaneous adsorption of TEC, AMO, and CIP onto CPS (initial antibiotic concentration = 60 mg/L, CPS dose = 0.1 g/100 mL, agitation time = 120 min, agitation speed = 150 rpm, and pH = 5).

Adsorbate	T (°C)	q_e (mg/g)	Thermodynamic parameters		
			ΔG° (kJ/mol)	ΔH° (kJ/mole)	ΔS° (kJ/mole K)
AMO	25	47.570	−3380.260	−30.347	−90.498
	30	46.192	−2927.734		
	35	43.191	−2475.250		
TEC	25	55.744	−5861.166	−86.033	−269.030
	30	53.383	−4516.001		
	35	51.863	−3170.836		
CIP	25	58.150	−5824.924	−38.415	−109.362
	30	56.212	−5278.114		
	35	53.541	−4731.304		

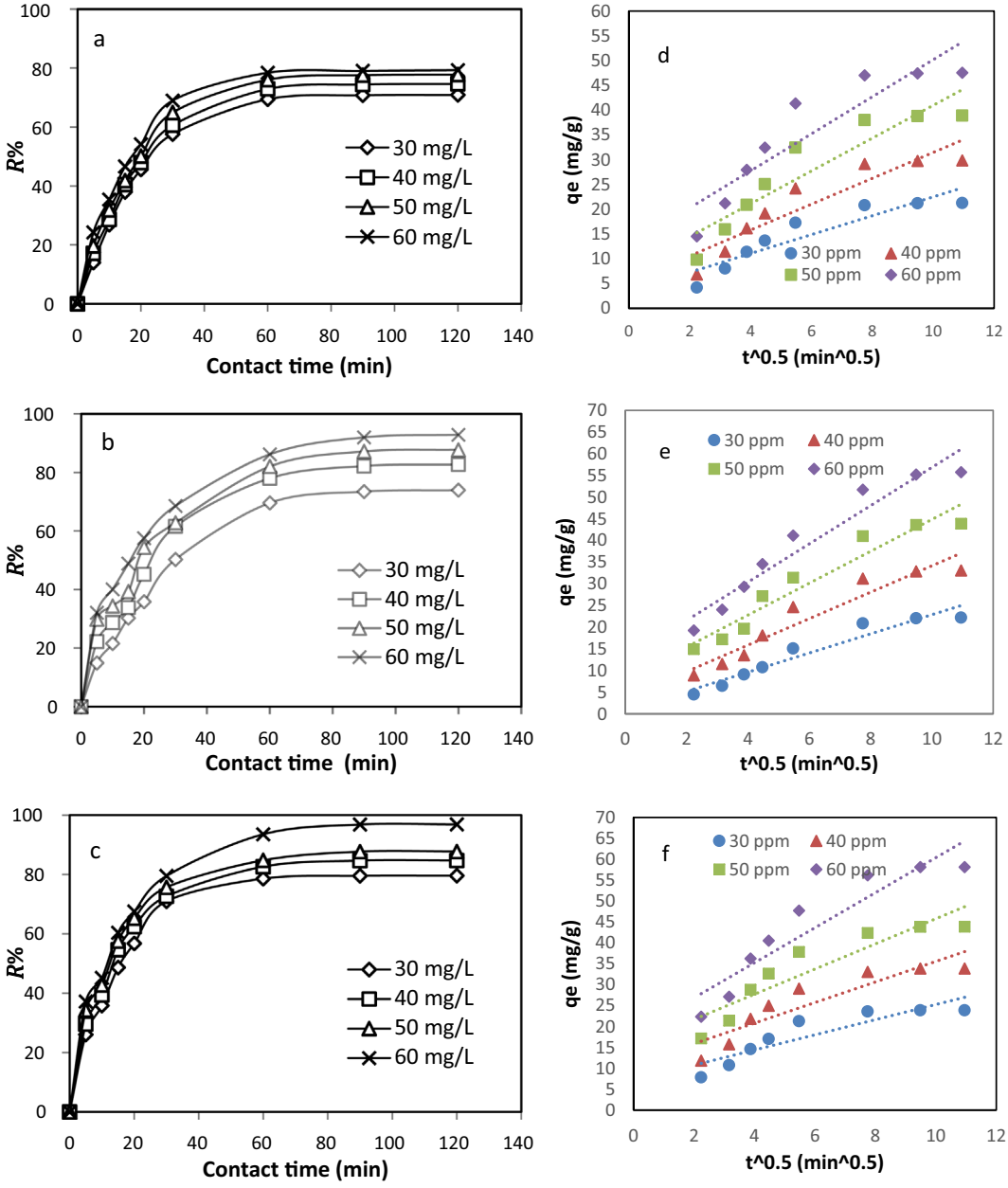

Fig. 9 Effect of initial TEC (a), AMO (b), and CIP (c) concentrations on their adsorption efficiency in the ternary system, and results of the application of intra-particle diffusion model of TEC (d), AMO (e), and CIP (f) adsorption data onto CPS.

Table 2 The kinetic model parameters and coefficients of regression for simultaneous TEC, AMO, and CIP adsorption onto CPS, where q_e,exp. and q_e,cal. are denoted by the q_e values that are determined experimentally and calculated using the kinetic model, respectively.

Adsorbate	C_0 (mg/L)	q_e exp. (mg/g)	Pseudo-first order			Pseudo-second order			Intra-particle diffusion		
			k_1 (min^{-1})	q_e cal. (mg/g)	R^2	k_2 (g/mg min)	q_e cal. (mg/g)	R^2	k_{id}	C	R^2
AMO	30	22.19	0.0564	27.93	0.9855	0.00117	27.01	0.9905	2.2097	0.77	0.9313
	40	33.09	0.0561	40.11	0.9874	0.00109	38.33	0.9898	3.0495	3.67	0.9147
	50	43.87	0.0541	47.05	0.9775	0.00108	45.59	0.9931	3.6767	8.07	0.9275
	60	55.74	0.0487	50.05	0.9854	0.00102	55.00	0.9992	4.41	12.74	0.9356
TEC	30	21.26	0.0716	27.77	0.9966	0.00208	24.91	0.9899	1.9049	3.448	0.8472
	40	29.85	0.0662	35.02	0.9983	0.00163	31.39	0.9990	2.6106	5.3569	0.8557
	50	37.9	0.0666	45.18	0.9484	0.00138	39.99	0.9937	3.3125	7.8523	0.853
	60	48.35	0.068	45.18	0.9878	0.00148	48.01	0.9906	3.7397	12.786	0.8306
CIP	30	23.89	0.085	31.00	0.9909	0.00330	26.10	0.9966	1.8126	7.1177	0.8114
	40	33.889	0.0818	40.08	0.9654	0.00250	36.16	0.9992	2.4593	10.96	0.8255
	50	43.88	0.0793	53.11	0.9462	0.00220	47.09	0.9981	3.0106	15.66	0.8355
	60	58.14	0.0809	80.92	0.9427	0.00140	64.51	0.9981	4.1911	18.458	0.8767

the data were evaluated with the intra-particle diffusion model (Eq. (8)). This model is often used to determine if intra-particle diffusion is the dominant rate-limiting step or there is another process like film, surface, or pore diffusion that can control the kinetics of the process (Boparai et al., 2011; Ozcan et al., 2007). According to Eq. (8), in case the linear trend linefit of q_t versus $t^{0.5}$ point passes through or is close to the origin point (i.e., the parameter $C \approx 0$), then the intra-particle diffusion is the sole rate-limiting step in the adsorption kinetic. Therefore, the kinetic data of TEC, AMO, and CIP adsorption onto CPS at different initial concentrations is plotted according to the intra-particle diffusion equation (Eq. (8)) and the results are presented in Fig. 9 (d to f). These figures show that the plots of the kinetic data, according to the intra-particle diffusion equation, are not fitted to the linear equations. In addition, all the calculated C values are higher than zero. This finding indicates that the adsorption process of TEC, AMO, and CIP onto CPS is controlled by more than one mechanism of adsorption and intra-particle diffusion is not the dominant mechanism in the adsorption process.

$$q_t = q_e\left(1 - e^{-k_1 t}\right) \tag{6}$$

$$q_t = \frac{k_2 q_e^2 t}{1 + k_2 q_e t} \tag{7}$$

$$q_t = k_{id} t^{0.5} + C \tag{8}$$

where $q_t q_t$ (mg/g) is the amount of each molecule of TEC, AMO, and CIP adsorbed onto the CPS at time t (min); k_1 and k_2 (min^{-1}) are the rate constants of the first- and second-order kinetic models; k_{id} (mg/g $min^{0.5}$) stands for the constant of the intra-particle diffusion rate, and C (mg/g) is a constant that gives information about the boundary layer thickness and is the controlling step of the adsorption process.

3.2.4.1. Effects of CPS dose and isotherm study. From an economic perspective, the determination of an optimum adsorbent dose is one of the crucial factors that must be found in adsorption process studies. Therefore, in the present study the effect of the adsorbent dose is studied within the range of CPS content of 0.02–0.1 g in 100 mL of 60 mg/L antibiotic solution (Fig. 10). It can be seen that with an increase in the CPS dose from 0.02 to 0.06 g/100 mL, the adsorption efficiency of TEC, AMO, and CIP proportionately increases. The reason behind this behavior with the rise in the adsorbent amount in the aqueous solution is the increase in the surface area or active sites for reaction of the pollutant molecules. In case of an increase in the adsorbent dose above 0.06 g/100 mL, the removal efficiencies are not altered greatly. The agglomeration of some CPS magnetic nanoparticles at high doses in the solution is the factor behind the decrease in the percentage of removal rate, due to the aggregation of the available active groups of the used adsorbent (Bazrafshan et al., 2019). Moreover, the recorded sequence of the removal efficiencies in the pH study is not altered here and is still at the rank of CIP > TEC > AMO for all the studied values of the adsorbent dose.

Langmuir (Eq. (9)) and Freundlich (Eq. (10)) isotherm models were used to simulate the experimental equilibrium

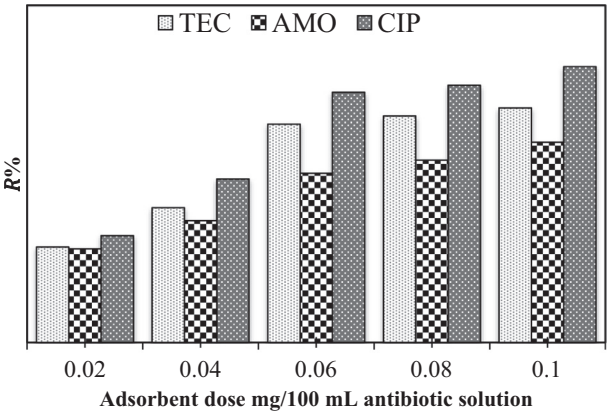

Fig. 10 Effect of CPS dose on the TEC, AMO, and CIP adsorption efficiency in the ternary system (initial antibiotic concentration = 60 mg/L, temperature = 25 ± 2 °C, contact time from 0 to 120 min, agitation speed = 150 rpm, and pH = 5).

Table 3 Calculated isotherm and regression parameters of the TEC, CIP, and AMO onto CPS.

Model	Parameter	TEC	CIP	AMO
Langmuir	q_{max} (mg/g)	92.450	98.717	132.24
	K_L (L/mg)	0.146	0.149	0.103
	R_L	0.102	0.1	0.139
	R^2	0.995	0.989	0.997
Freundlich	k_f (mg/g)	33.382	33.176	26.66
	$1/n$	4.233	3.848	2.56
	R^2	0.997	0.995	0.989

data. In recent times, these two models have been widely used in published articles with regard to modeling of the experimental isotherm data of different adsorbents (Khodadadi et al., 2019; Martins et al., 2015; Sulaymon et al., 2014).

$$q_e = \frac{q_{max} K_L C_e}{1 + K_L C_e} \tag{9}$$

$$q_e = K_f C_e^{\frac{1}{n}} \tag{10}$$

$$R_L = \frac{1}{(1 + K_L C_0)} \tag{11}$$

where q_{max} is an essential parameter representing the maximum adsorption capacity of the adsorbent (mg/g), and K_L is a Langmuir constant denoting the affinity of the adsorbent's active sites (L/mg), n is a parameter of the Freundlich equation (g/L) related to sorption intensity, in which the desirability of the adsorption process can be specified in case of $\frac{1}{n} < 1$, and K_f is the Freundlich constant related to the relative sorption capacity (mg/g).

The models constants and correlation coefficients were calculated using non-linear regression; the results are presented in Table 3. Besides, Fig. 11 displayed the plot of the obtained theoretical and experimental data. It is remarkable that the adsorption data of both TEC and CIP on CPS have adjusted well to the Freundlich model, in which the adequate correlation coefficient values were determined. On the other hand, the Langmuir isotherm model was found to be the better model to describe AMO adsorption onto CPS. These findings were enlightening a complex mechanism of simultaneous antibiotic adsorption onto the adsorbent's surface, wherein the CIP surfaces comprise of different adsorption sites; therefore, each antibiotic reacted differently from the other with the CIP. The TEC and CIP molecules reacted on a multi-layer and heterogeneous active sites of the surface of CPS, whereas, the adsorption of AMO molecules were characterized by a monolayer adsorption type that occurred on a homogeneous CPS surface. The maximum adsorption uptakes, based on Langmuir model analysis, were high, and found to be 92.45, 98.717, and 132.240 mg/g for TEC, CIP, and AMO, respectively. In addition, the results of the best-fit model, represented by n values of TEC and CIP adsorption and the R_L value of AMO, determined using Eq. (11), indicated that the adsorption process using CIP adsorbent was favored. As the n values were determined to be <1, a chemisorption process was involved for the three antibiotic adsorptions onto CIP (Aljeboree et al., 2017; Kumar et al., 2010). These results were quite consistent with our findings in the kinetic study. In addition, Table 4 lists the maximum uptakes for TEC, CIP, and

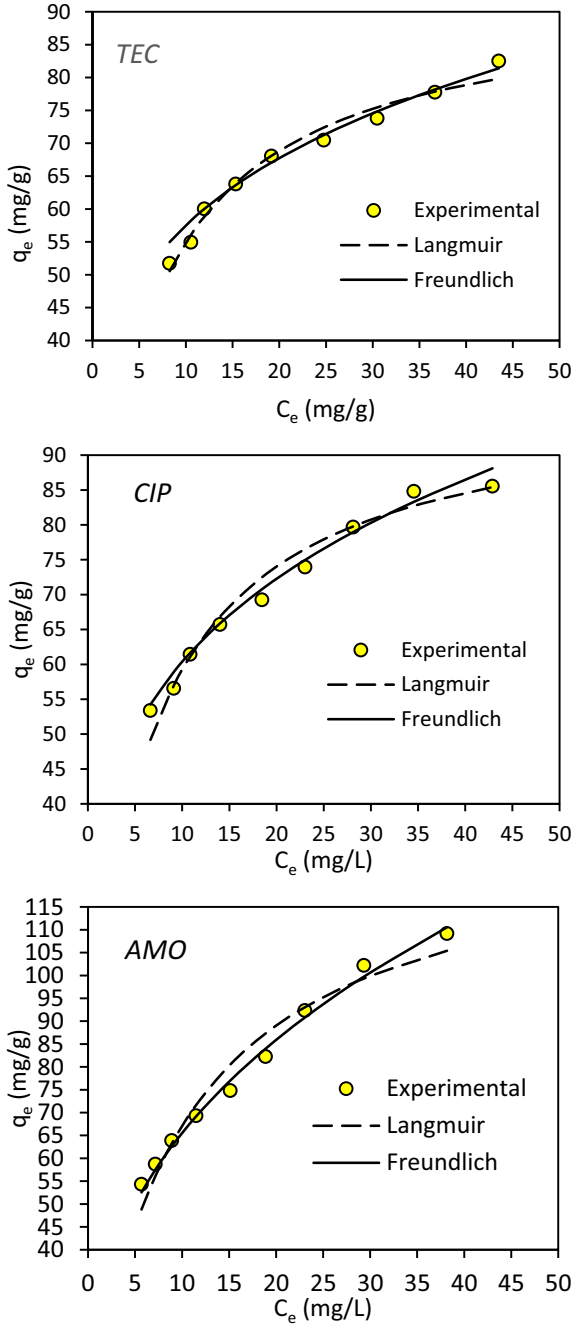

Fig. 11 A graph showing the experimental and theoretical isotherm values of TEC, CIP, and AMO onto CPS.

Table 4 The comparison of the adsorption efficiency of CPS with other adsorbents for the antibiotic adsorption from aqueous solutions.

Adsorbent	q_{max}(mg/g)	Reference
TEC		
The red soil	12.00	Wang et al., (2010)
HCl-modified zeolite	20.40	Zou et al., (2012)
Bamboo charcoal	23.50	Liao et al., (2013)
Hydroxyapatite/clay	76.02	Ersan et al., (2015)
Nanosheet-layered double hydroxide	98.04	Soori et al., (2016)
CPS	98.71	This study
CIP		
Corylus avellana (hazelnut) activated carbon	73.64	Balarak et al., (2016)
ZnO nanoparticles	8.30	Dhiman and Sharma (2018)
Groundnut (Arachis hypogaea) shell powder	8.86	Dhiman and Sharma (2018)
MgO nanoparticles	3.46	Khoshnamvand et al., (2017)
Magnetic activated carbon/chitosan	90.00	Danalıoğlu et al., (2017)
CPS	92.45	This study
AMO		
Almond shell	2.50	Homem et al., (2010)
MNPs-PAC	142.85	Kakavandi et al., (2013)
Chitosan beads	8.71	Adriano et al., (2005)
Olive stone activated carbon	57.00	Limousy et al., (2016)
Magnetically modified grapheme nano-platelets	14.10	Kerkez-Kuyumcu et al., (2016)
CPS	132.24	This study

AMO adsorption using current adsorbent and other studied materials that taken under investigation in previous works. Based on the results presented in this table, the CPS exhibited high performance toward elimination of antibiotic molecules in the adsorption treatment process when compared with other adsorbens.

4. Conclusions

The present study has investigated the adsorptive performance of the CPS toward TEC, AMO, and CIP adsorption in the ternary system. The CPS adsorbent was characterized by advanced means of TEM, SEM, XRD, and FT-IR. The results of the characterization study demonstrated that the coating process of the pistachio shell by ZnO nanoparticles had positive effects on the prepared adsorbent, in terms of practical utilization and adsorption ability. In addition, the parameters of the adsorption process were optimized with the variation in values of pH, contact time, initial antibiotic concentration, temperature, and CPS dose. From the optimized data of the effect study, the isotherm, kinetic, and thermodynamic studies were accomplished. The isotherm data of AMO adsorption could be predicted using the Langmuir model, while the TEC and CIP isotherm data followed the Fruendlich model. Thus, the isotherm study showed that the surface of CPS comprised of both heterogeneous and homogeneous adsorption sites that were ready for reaction with antibiotic molecules. The thermodynamic parameters highlighted that the nature of the simultaneous adsorption process was spontaneous and exothermic. The CPS maximum adsorption capacity based on the Langmuir model results for the three antibiotics could be ranked as: AMO > CIP > TEC. The kinetic data of the three antibiotics are adequately modeled by the pseudo-second-order model, indicating that the nature of the kinetic adsorption is chemical. In addition, the kinetic study showed that there was more than one process that controlled the kinetic rate. The present study shows CPS to be an effective adsorbent, which can be used for the sequestration of antibiotics in the adsorption treatment systems. In the future studies, it is recommended to identify the magnetic force of CPS and the effect of agitation speed on the adsorption performance of CPS.

Acknowledgments

The researchers appreciate the scientific cooperation between the University of Baghdad (Iraq) and the IsraUniversity (Jordan). Also, a special thanks to GlobalEdico (India) for their valuable efforts to edit and improve the English language of this research.

References

Abdelwahab, N.A., Ghoneim, A.M., 2018. Photocatalytic activity of ZnO coated magnetic crosslinked chitosan/polyvinyl alcohol microspheres. Mater. Sci. Eng., B 228, 7–17.

Adriano, W.S., Veredas, V., Santana, C.C., Gonçalves, L.R.B., 2005. Adsorption of amoxicillin on chitosan beads: Kinetics, equilibrium and validation of finite bath models. Biochem. Eng. J. 27 (2), 132–137.

Ahalya, N., Ramachandra, T.V., Kanamadi, R.D., 2003. Biosorption of Heavy Metals. Res. J. Chem. Environ 7 (4), 71–79.

Aljeboree, A.M., Alshirifi, A.N., Alkaim, A.F., 2017. Kinetics and equilibrium study for the adsorption of textile dyes on coconut shell activated carbon. Arabian J. Chem. 10, S3381–S3393.

Al-Musawi, T.J., Brouers, F., Zarrabi, M., Noroozi, R., 2018. What can the use of well-defined statistical functions of pollutants sorption kinetics teach us? A case study of cyanide sorption onto LTA zeolite nanoparticles. Environ. Technol. Innov. 10, 46–54.

Al-Musawi, T.J., Kamani, H., Bazrafshan, E., Panahi, A.H., Silva, M. F., Abi, G., 2019. Optimization the effects of physicochemical parameters on the degradation of cephalexin in sono-fenton reactor by using box-behnken response surface methodology. Catal. Lett. 149 (5), 1186–1196.

Arami, M., Limaee, N.Y., Mahmoodi, N.M., Tabrizi, N.S., 2005. Removal of dyes from colored textile wastewater by orange peel adsorbent: Equilibrium and kinetic studies. J Colloid Interface Sci. 288, 371–376.

Balarak, D., Mostafapour, F.K., Azarpira, H., 2016. Adsorption kinetics and equilibrium of ciprofloxacin from aqueous solutions using corylus avellana (Hazelnut) activated carbon. Brit. J. Pharm. Res. 13 (3), 1–14.

Balcioglu, I.A., Otker, M., 2004. Pre-Treatment of Antibiotic Formulation Wastewater by O_3, O_3/H_2O_2, and O_3/UV Processes. Turk. J. Eng. Environ. Sci. 28 (5), 325–332.

Bazrafshan, E., Al-Musawi, T.J., Silva, M.F., Panahi, A.H., Havangi, M., Mostafapur, F.K., 2019. Photocatalytic degradation of cate-

chol using ZnO nanoparticles as catalyst: Optimizing the experimental parameters using the Box-Behnken statistical methodology and kinetic studies. Microchem. J. 147, 643–653.

Binh, V.N., Dang, N., Anh, N.T.K., Ky, L.X., 2018. Thai P.K., Antibiotics in the aquatic environment of Vietnam: Sources, concentrations, risk and control strategy. Chemosphere 197, 438–450.

BIO Intelligence Service, 2013. Study on the environmental risks of medicinal products, Final Report prepared for Executive Agency for. Health Consum.

Bondarczuk, K., Piotrowska-Seget, Z., 2019. Microbial diversity and antibiotic resistance in a final effluent-receiving lake. Sci. Total Environ. 650, 2951–2961.

H.K. Boparai M. Joseph D.M. O'Carroll Kinetics and thermodynamics of cadmium ion removal by adsorption onto nanozerovalent iron particles, J. Hazard. Mater. 2011, 186: (1): 458-465.

Brouers, F., Al-Musawi, T.J., 2018. Brouers-Sotolongo fractal kinetics versus fractional derivative kinetics: a new strategy to analyze the pollutants sorption kinetics in porous materials. Hazard. Mat. 350, 162–168.

Changsuphan, A., Wahab, M., Oanh, N., 2012. Removal of benzene by ZnO nanoparticles coated on porous adsorbents in presence of ozone and UV. Chem. Eng. J. 181–182, 215–221.

Chen, Z.X., Jin, X.Y., Chen, Z., Megharaj, M., Naidu, R., 2011. Removal of methyl orange from aqueous solution using bentonite-supported nanoscale zero-valent iron. J. Colloid Interface Sci. 363, 601–607.

Cheng, M., Zhang, X., Shi, Y., Shi, D., Zhu, G., Fan, J., 2019. Highly efficient removal of ceftiofur sodium using a superior hydroxyl group functionalized ionic liquid-modified polymer. Sci. Total Environ. 662, 324–331.

Danalıoğlu, S.T., Bayazit, Ş.S., Kerkez Kuyumcu, Ö., Salam, M.A., 2017. Efficient removal of antibiotics by a novel magnetic adsorbent: Magnetic activated carbon/chitosan (MACC) nanocomposite. J. Mol. Liq. 240, 589–596.

Davis, A., Volesky, B., Mucci, A., 2003. A review of the biochemisty of heavy metals biosorption by brown algae. Water Res. 37, 4311–4330.

Dhiman, N., Sharma, N., 2018. Batch adsorption studies on the removal of ciprofloxacin hydrochloride from aqueous solution using ZnO nanoparticles and groundnut (Arachis hypogaea) shell powder: a comparison. Indian Chem. Eng., 1–10.

Ersan, M., Guler, U.A., Acıkel, U., Sarioglu, M., 2015. Synthesis of hydroxyapatite/clay and hydroxyapatite/pumice composites for tetracycline removal from aqueous solutions. Process Saf. Environ. Prot. 96, 22–32.

Gasser, M.S., Mohsen, H.T., Aly, H.F., 2008. Humic acid adsorption onto Mg/Fe layered double hydroxide, Colloids and Surfaces A: Physicochem. Eng. Aspects 331, 195–201.

Ghadim, E.E., Manouchehri, F., Soleimani, G., Hosseini, H., et al, 2013. Adsorption properties of tetracycline onto graphene oxide: equilibrium. Kinetic Thermodyn. Stud. 8 (11), 1–9.

Ghaseminasab, P.M., Ahmadi, A., Mazloomi, S.M., 2015. A review on pistachio: Its composition and benefits regarding the prevention or treatment of diseases. JOHE 4 (1), 57–69.

Ghorai, S., Sarkar, A.K., Pal, S., 2014. Rapid adsorptive removal of toxic Pb^{2+}, ion from aqueous solution using recyclable, biodegradable nanocomposite derived from templated partially hydrolyzed xanthan gum and nanosilica. BioresourTechnol. 170 (5), 578–582.

Gisi, S.D., Lofrano, G., Grassi, M., Notarnicola, M., 2016. Characteristics and adsorption capacities of low-cost sorbents for wastewater treatment: A review. Sustain. Mater.Technol. 9, 10–40.

Gupta, V.K., Agarwal, S., Asif, M., Fakhri, A., Sadeghi, N., 2017. Application of response surface methdology to optimize the adsorption performance of a magnetic graphene oxide nanocomposite adsorbent for removal of methadone from the environment. J. Colloid Interface Sci. 497, 193–200.

Handore, K., Bhavsar, S., Horne, A., Chhattise, P., Mohiteb, K., et al, 2014. Novel green route of synthesis of ZnO nanoparticles by using natural biodegradable polymer and its application as a catalyst for oxidation of aldehydes. J. Macromol. Sci., Part A: Pure Appl. Chem. 51, 941–947.

Hashemian, S., Shayegan, J., 2014. A comparative study of cellulose agricultural wastes (almond shell, pistachio shell, walnut shell, tea waste and orange peel) for adsorption of violet B dye from aqueous solutions. Orient. J. Chem. 30 (4), 2091–2098.

Hassani, A., Torabian, A., Rahimi, K., 2014. Performance of iron-zero (nZVI) nanno particles in removal of cephalexin from synthetic wastewater. J Water Wastewater 25, 85–92.

Holan, Z.R., Volesky, B., 1995. Accumulation of cadmium, lead and nickel by fungal and wood biosorbents. Appl. Biochem. Biotechnol. 53, 133–142.

Homem, V., Alves, A., Santos, L., 2010. Amoxicillin removal from aqueous matrices by sorption with almond shell ashes. Int. J. Environ. Anal. Chem. 90 (14–15), 1063–1084.

Hossain, M.A., Ngo, H.H., Guo, W.S., Setiadi, T., 2012. Adsorption and desorption of copper(II) ions onto garden grass. J. Bioresour. Technol. 121, 386–395.

Hsu, L.G., Liu, Y.-T., Syu, C.H., Huang, M.H., Tzou, Y.-M., Teah, H.Y., 2018. Adsorption of tetracycline on Fe (hydroxides): effects of pH and metal cation (Cu^{2+}, Zn^{2+} and Al^{3+}) addition in various molar ratios. R. Soc. Open Sci. 5, 171941. https://doi.org/10.1098/rsos.171941. eCollection 2018 Mar.

Huang, X., Zheng, J., Liu, C., Liu, L., Liu, Y., Fan, H., 2017. Removal of antibiotics and resistance genes from swine wastewater using vertical flow constructed wetlands: Effect of hydraulic flow direction and substrate type. Chem. Eng. J. 308, 692–699.

Jeong, B., Kim, D.H., Park, E.J., Jeong, M.-G., Kim, K.-D., Seo, H. O., Kim, Y.O., Uhm, S., 2014. ZnO shell on mesoporous silica by atomic layer deposition: Removal of organic dye in water by an adsorbent and its photocatalytic regeneration. Appl. Surf. Sci. 307, 468–474.

Ji, Y., Ferronato, C., Salvador, A., Yang, X., Chovelon, J.-M., 2014. Degradation of ciprofloxacin and sulfamethoxazole by ferrousactivatedpersulfate: implications for remediation of groundwater contaminated by antibiotics. Sci Total Environ. 472, 800–808.

Joshi, R., 2018. Facile photochemical synthesis of ZnO nanoparticles in aqueous solution without capping agents. Materialia 2, 104–110.

Kakavandi, B., Esrafili, A., Mohseni-Bandpi, A., Jonidi Jafari, A., Rezaei Kalantary, R., 2013. Magnetic Fe_3O_4@C nanoparticles as adsorbents for removal of amoxicillin from aqueous solution. Water Sci. Technol. 69 (1), 147–155.

Kalhori, E.M., Ghahramani, E., Al-Musawi, T.J., Saleh, H.N., Sepehr, M.N., Zarrabi, M., 2018. Effective reduction of metronidazole over the cryptomelane-type manganese oxide octahedral molecular sieve (K-OMS-2) catalyst: facile synthesis, experimental design and modeling, statistical analysis, and identification of by-products. Environ. Sci. Pollut. Res. 25, 34164–34180.

Kamar, F.H., Nechifor, A.C., Nechifor, G., Al-Musawi, T.J., Mohammed, A.H., 2017. Aqueous Phase Biosorption of Pb(II), Cu(II), and Cd(II) onto Cabbage Leaves Powder. Int. J. Chem. Reactor Eng. 15 (2). https://doi.org/10.1515/ijcre-2015-0178.

Kerkez-Kuyumcu, Ö., Bayazit, Ş.S., Salam, M.A., 2016. Antibiotic amoxicillin removal from aqueous solution using magnetically modified graphene nanoplatelets. J. Ind. Eng. Chem. 36, 198–205.

Khodadadi, M., Al-Musawi, T.J., Kamranifar, M., Saghi, M.H., Panahi, A.H., 2019. A comparative study of using barberry stem powder and ash as adsorbents for adsorption of humic acid. Environ. Sci. Pollut. Res. https://doi.org/10.1007/s11356-019-05879-4.

Khoshnamvand, N., Ahmadi, S., Mostafapour, F.K., 2017. Kinetic and isotherm studies on ciprofloxacin an adsorption using magnesium oxide nanopartices. J. Appl. Pharm. Sci. 7 (11), 79–83.

Kumar, H., Rani, R., 2013. Structural and optical characterization of ZnO nanoparticles synthesized by microemulsion route. Int. Lett. Chem., Phys. Astron. 14, 26–36.

Kumar, P.S., Ramalingam, S., Senthamarai, C., Niranjanaa, M., Vijayalakshmi, P., Sivanesan, S., 2010. Adsorption of dye from aqueous solution by cashewnut shell: studies on equilibriumisotherm, kinetics and thermodynamics of interactions. Desalination 261, 52–60.

Legnoverde, M.S., Simonetti, S., Basaldella, E.I., 2014. Influence of pH on cephalexin adsorption onto SBA-15 mesoporous silica: Theoretical and experimental study. Appl. Surf. Sci. 300, 37–42.

Li, Z., Huang, Y., Wang, H., Wang, D., Wang, X., Han, F., 2017. Three-dimensional hierarchical structures of ZnO nanorods as a structure adsorbent for water treatment. J. Mater. Sci. Technol. 33, 864–868.

Liao, P., Zhan, Z., Dai, J., Wu, X., Zhang, W., Wang, K., Yuan, S., 2013. Adsorption of tetracycline and chloramphenicol in aqueous solutions by bamboo charcoal: a batch and fixed-bed column study. Chem. Eng. 228, 496–505.

Lien, L., Hao, N., Chuc, N., et al, 2016. Antibiotics in wastewater of a rural and an urban hospital before and after wastewater treatment, and the relationship with antibiotic use—A one year study from Vietnam. Int J Environ Res Public Health 13 (6), 588.

Limousy, L., Ghouma, I., Ouederni, A., Jeguirim, M., 2016. Amoxicillin removal from aqueous solution using activated carbon prepared by chemical activation of olive stone. Environ. Sci. Pollut. Res. 24 (11), 9993–10004.

Martins, A.C., Pezoti, O., Cazetta, A.L., Bedin, K.C., Yamazaki, D. A., Bandoch, G.F., Asefa, T., Visentainer, J.V., Almeida, V.C., 2015. Removal of tetracycline by NaOH-activated carbon produced from macadamianut shells: kinetic and equilibrium studies. Che. Eng. J. 260, 291–299.

Mohammed, A.A., Brouers, F., Samaka, I.S., Al-Musawi, T.J., 2018. Role of Fe_3O_4 magnetite nanoparticles used to coat bentonite in zinc(II) ions sequestration. Environ. Nanotechnol. Monit. Manage. 10, 17–27.

Mohammed, A.A., Kareem, S.L., 2019. Adsorption of tetracycline fom wastewater by using Pistachio shell coated with ZnO nanoparticles: Equilibrium, kinetic and isotherm studies. Alexandria Engineering Journal.

Mohammed, A.A., Najim, A.A., Al-Musawi, T.J., Alwared, A.I., 2019. Adsorptive performance of a mixture of three nonliving algae classes for nickel remediation in synthesized wastewater. J. Environ. Health Sci. Eng. https://doi.org/10.1007/s40201-019-00367-w.

Mohseni-Bandpi, A., Al-Musawi, T.J., Ghahramani, E., Zarrabi, M., Mohebi, S., Vahed, S.A., 2016. 2016, Improvement of zeolite adsorption capacity for cephalexin by coating with magnetic Fe_3O_4 nanoparticles. J. Mol. Liq. 218, 615–624.

Noroozi, N., Al-Musawi, T., Kazemian, H., Kalhori, H.E., Zarrabi, M., 2018. Removal of cyanide using surface-modified Linde type-A zeolite nanoparticles as an efficient and ecofriendly material. Water Process Eng. 21, 44–51.

Oh, W.-D., Chang, V., Lim, T.-T., 2017. A comprehensive performance evaluation of heterogeneous Bi2Fe4O9/peroxymonosulfate system for sulfamethoxazole degradation. Environ. Sci. Pollut. Res. https://doi.org/10.1007/s11356-017-8476-9.

Ozcan, A., Ozcan, A.S., Gok, O., 2007. Adsorption kinetics and isotherms of anionic dye of reactive blue 19 from aqueous solutions onto DTMA-sepiolite. In: Lewinsky, A.A. (Ed.), Hazardous Materials and Wastewater—Treatment, Removal and Analysis. Nova Science Publishers, New York.

Piness, J., 2010. Physical and chemical structural analysis of pistachio shells. J. Undergrad. Mater. Res. 4. https://doi.org/10.21061/jumr.v4i0.1564.

Pouretedal, H.R., Sadegh, N., 2014. Effective removal of amoxicillin, cephalexin, tetracycline and penicillin G from aqueous solutions using activated carbon nanoparticles prepared from vine wood. J. Water Process. Eng. 1, 64–73.

Qu, F., Morais, P.C., 2001. The pH dependence of the surface charge density in oxide-based semiconductor nanoparticles immersed in aqueous solution. IEEE Trans. Magn. 37, 2654–2656.

Qu, F., Morais, P.C., 1999. Energy levels in metal oxide semiconductor quantum dots in waterbased colloids. J. Chem. Phys. 111, 8588–8594.

Rana, S.B., Bhardwaj, V.K., Singh, S., Singh, A., Kaur, N., 2012. Influence of surface modification by 2-aminothiophenol on optoelectronics properties of ZnO nanoparticles. J. Exp. Nanosci., 1–15

Samarghandi, M., Al-Musawi, T., Mohseni-Bandpi, A., Zarrabi, M., 2015. Adsorption of cephalexin from aqueous solution using natural zeolite and zeolite coated with manganese oxide nanoparticles. J. Mo. Liq. 2015 (211), 431–441.

Sharma, P.C., Jain, A., Jain, S., 2009. Fluoroquinoloneantibacterials: a review on chemistry, microbiology and therapeutic prospects. Acta PoloniaePharmaceutica -Drug Res. 66, 587–604.

Shi, Z.-Q., Liu, Y.-S., Xiong, Q., Cai, W.-W., Ying, G.-G., 2019. Occurrence, toxicity and transformation of six typical benzotriazoles in the environment: A review. Sci. Total Environ. 661, 407–421.

Soori, M.M., Ghahramani, E., Kazemian, H., Al-Musawi, T.J., Zarrabi, M., 2016. Intercalation of tetracycline in nano sheet layered double hydroxide: an insight into UV/VIS spectra analysis. J. Taiwan Ins. Chem. Eng. 67, 271–285.

Stuart, B., 2004. Infrared spectroscopy: fundamentals and applications. Wiley, Sussex.

Sulaymon, A., Mohammed, A., Al-Musawi, T., 2014. Comparative study of removal of cadmium (II) and chromium (III) ions from aqueous solution using low-cost biosorbent. Int. J. Chem. Reac. Eng. 12 (1), 1–10.

Sun, Y., Li, H., Li, G., Gao, B., Yue, Q., Li, X., 2016. Characterization and ciprofloxacin adsorption properties of activated carbons prepared from biomass wastes by H_3PO_4 activation. Bioresour. Technol. 217, 239–244. https://doi.org/10.1016/j.biortech.2016.03.047.

Wang, J., Zhang, T., Li, M., Yang, Y., Lu, P., Ning, P., Wang, Q., 2018. Arsenic removal from water/wastewater using layered double hydroxide derived adsorbents, a critical review. RSC Adv. 8, 22694–22709.

Wang, L., Han, C., Nadagouda, M.N., Dionysiou, D.D., 2016. An innovative zinc oxide-coated zeolite adsorbent for removal of humic acid. J. Hazard. Mater. 313, 283–290.

Wang, Y., Sun, R., Xiao, A., Wang, S., Zhou, D., 2010. Phosphate affects the adsorption of tetracycline on two soils with different characteristics. Geoderma 156 (3–4), 237–242.

Wu, Q., Li, Z., Hong, H., Yin, K., Tie, L., 2010. Adsorption and intercalation of ciprofloxacin on montmorillonite. Appl. Clay Sci. 50 (2), 204–211. https://doi.org/10.1016/j.clay.2010.08.001.

Xian, Q., Hu, L., Chen, H., Chang, Z., Zou, H., 2010. Removal of nutrients and veterinary antibiotics from swine wastewater by a constructed macrophyte floating bed system. J. Environ. Manage. 91, 2657–2661.

Zou, C., Jiang, W., Liang, J., Sun, X., Guan, Y., 2019. Removal of Pb (II) from aqueous solutions by adsorption on magnetic bentonite. Environ. Sci. Pollut. Res. 26, 1315–1322. https://doi.org/10.1007/s11356-018-3652-0.

Zhang, F., Chen, X., Wu, F., Ji, Y., 2016. High adsorption capability and selectivity of ZnO nanoparticles for dye removal. Colloids Surf., A 509, 474–483.

Zou, Y.L., Huang, H., Chu, M., Lin, J.W., Yin, D.Q., Li, Y.N., 2012. Adsorption research of tetracycline from water by HCl-modified zeolite. Adv. Mater. Res. 573–574, 43–47.